Arctic stratus cloud properties and their effect on the surface radiation budget; Selected cases from FIRE ACE

Xiquan Dong,[1] Gerald G. Mace, [1] Patrick Minnis, [2] David F. Young, [2]

Short title: DONG ET AL.: ARCTIC STRATUS CLOUD PROPERTIES AND FEEDBACKS

Abstract.

To study Arctic stratus cloud properties and their effect on the surface radiation balance during the spring transition season, analyses are performed using data taken during 3 cloud and 2 clear days in May 1998 as part of the First ISCCP Regional Experiment (FIRE) Arctic Cloud Experiment (ACE). Radiative transfer models are used in conjunction with surface- and satellite-based measurements to retrieve the layer-averaged microphysical and shortwave radiative properties. The surface-retrieved cloud properties in Cases 1 and 2 agree well with the in situ and satellite retrievals. Discrepancies in Case 3 are due to spatial mismatches between the aircraft and surface measurements in a highly variable cloud field. Also, the vertical structure in the cloud layer is not fully characterized by the aircraft measurements. Satellite data are critical for understanding some of the observed discrepancies. The satellite-derived particle sizes agree well with the coincident surface retrievals and with the aircraft data when they were collocated. Optical depths derived from visible-channel data over snow backgrounds were overestimated in all three cases suggesting that methods currently used in satellite cloud climatologies derive optical depths that are too large. Use of a near-infrared channel with a solar infrared channel to simultaneously derive optical depth and particle size appears to alleviate this overestimation problem. Further study of the optical depth retrieval is needed. The surface-based radiometer data reveal that the Arctic stratus clouds produce a net warming of 20 $\mathrm{W\,m^{-2}}$ in the surface layer during the transition season suggesting that these clouds may accelerate the spring time melting of the ice pack. This surface warming contrasts with the net cooling at the top of atmosphere (TOA) during the same period. An analysis of the complete FIRE ACE datasets will be valuable for understanding the role of clouds during the entire melting and refreezing process that occurs annually in the Arctic.

1. Introduction

Low-level stratiform clouds, due to their high albedo, have been widely recognized as having a strong cooling effect on the atmosphere-earth system from early theoretical studies [*Manabe and Wetherald,* 1967; *Schneider,* 1972] to later satellite observations [*Ramanathan et al.,* 1989; *Harrison et al.,* 1990; *Hartmann et al.,* 1992]. However, this result may not hold at the high latitudes because the albedo of snow/ice-covered surface is comparable to (or even higher than) the albedo of clouds. The effect of Arctic stratus clouds on the surface radiation budget is also complicated due to the presence of a highly reflecting surface. During the spring transition season, the thermodynamic balance is complicated because the low clouds tend to evolve from the predominately ice-phase clouds of winter to the liquid-phase clouds of summer. Thus, mixed phase clouds are common. Simultaneously, the high albedo surface of winter begins to melt and forms a mosaic of low albedo melt ponds interspersed with much higher albedo regions of ice. In the absence of clouds the evolving feedback processes in spring are conceptually straightforward with an accelerating warming and melting due to the ice-albedo interactions. Boundary layer clouds influence this positive feedback loop in either a positive or negative sense depending on their macro- and microphysical properties [*Stamnes et al.,* 1999]. *Curry et al.* [1996] used a 1D coupled atmosphere-sea ice model to evaluate cloud feedbacks to the surface, and conclude that the Arctic stratus cloud-radiation feedback is inextricably linked with the snow/ice albedo feedback. They show that on a yearly average, the clouds have a net warming effect on the surface. This result is opposite to that of stratus clouds of the middle latitudes.

To provide a much needed source of validation data for model results and satellite retrievals, as well as for improving climate model parameterizations, the First ISCCP(International Satellite Cloud Climatology Project) Regional Experiment (FIRE) Arctic Cloud Experiment (ACE) was conducted in a 3 x 3 degree latitude/longitude region from April to July, 1998 [*Curry et al.,* 2000]. FIRE ACE was conducted jointly

with the Surface Heat Budget of the Arctic Ocean (SHEBA) project [*Perovich et al.,* 1999] and the Atmospheric Radiation Measurement (ARM) program [*Stokes and Schwartz,* 1994]. The surface-based measurements at the SHEBA ice station, combined with the aircraft in situ measurements and satellite imagery can be used to study the stratus cloud properties and their effect on the surface radiation budget over the Arctic region. The aircraft in situ measurements can also serve as a "ground truth" data set for surface- and satellite-based retrievals of cloud microphysical properties. If the surface retrievals are verified, then they can be used in the future to provide more extensive verification of satellite-based cloud retrievals from sites such as the ARM North Slope of Alaska site in Barrow, Alaska. No validations of surface-derived cloud properties have been attempted yet for polar regions. In this paper, the Arctic stratus cloud macro- and microphysical properties, and their radiative feedbacks to the surface are studied from 3 selected cloudy cases on May 4/5, May 15/16, and May 27/28, 1998, respectively. The surface and aircraft results are also compared with satellite cloud property retrievals to begin the process of validating the passive remote sensing algorithms for polar applications. The aircraft instruments, and the surface- and satellite-based measurements and retrieval methods are described in section 2. The cloud macro- and microphysical properties are presented and compared in section 3. The surface radiation budget and stratus cloud-radiative feedbacks are discussed in section 4, and the conclusion is given in the last section.

2. Measurements and retrieval technique

The surface-based instruments were installed on or near the SHEBA ship that served as a floating science station and drifted from 76.013N, 165.357W to 76.556N, 168.004W from the early May to late May [*Curry et al.,* 2000; *Stamnes et al.,* 1999]. *Dong et al.* [1997, 1998, 2000] demonstrated that the combined measurements from the surface-based remote sensors, such as a radar, laser ceilometer, microwave radiometer,

and radiosonde, can be combined to yield information on liquid phase stratus cloud macro- and microphysical properties. The up- and down-looking standard Eppley precision spectral pyranometers (PSPs) and pyrgeometers provide measurements of downward and upward broadband solar (0.3 to 3 μm) and infrared (4 to 50 μm) fluxes at the surface. The surface albedo can be inferred from the ratio of upward to downward solar fluxes.

To retrieve the microphysical and radiative properties of stratus clouds, the approach described by *Dong et al.* [1997] (hereafter referred to as D97) has been applied. In the D97 scheme, a δ2-stream radiative transfer model is used in conjunction with surface-based measurements to retrieve the layer-averaged microphysical properties (cloud-droplet effective radius r_e and number concentration N). The derived radiative properties consist of broadband shortwave optical depth τ and cloud and TOA albedos. The retrieval scheme is based on an iterative approach that uses the liquid water paths LWP retrieved from microwave-radiometer-measured brightness temperatures and the cloud boundaries provided by laser ceilometer and cloud radar. The layer-averaged value of r_e in the radiative transfer calculations is adjusted until the model-computed solar flux at the surface matches the modified PSP-measured value. In the retrieval, the cloud droplets are assumed to have a lognormal size distribution with a logarithmic width of 0.35.

The measured downward solar fluxes were modified to account for the biases between the clear-sky measured and modeled surface downward solar fluxes [*Kato et al.,* 1997]. Based on clear sky measurements and model calculations near local noon we found the measured solar fluxes to be consistently lower by a factor of around 0.964. Therefore, we adjust the flux measurements on cloudy days by this amount. While this simple correction introduces some uncertainties in the cloudy results, the approach to this problem outlined by D97 is impossible to apply to the SHEBA data due to the lack of clear-sky information needed for determining the corrections. The uncertainties

in the retrieved cloud radiative properties were shown by *Dong et al.* [1997, 1998] to be generally less than 5%, while the errors in the retrieved r_e and N are about 15% and 30%, respectively. We expect these error figures to be slightly larger due to the correction we apply to the solar flux measurements.

The D97 technique was initially designed for single-layer, liquid phase stratus clouds. We will show that it is possible to apply the D97 method to mixed phase clouds when the liquid phase dominates the cloud microphysical and radiative properties. Since the D97 technique primarily relies on the microwave-radiometer-derived LWP and the PSP-measured solar flux, the differential effects of ice particles on the spectral measurements relative to the water droplet effects may be used to partition the amounts of ice and liquid water. Ice particles also have much smaller absorption coefficients than liquid water droplets and, therefore a very weak effect ($<< 1K$) on the brightness temperatures for non-precipitating clouds at microwave frequencies [*Lin et al.,* 1998]. Therefore, the microwave radiometer is not sensitive to ice particles and can provide accurate LWP retrievals in mixed phase cloud conditions. The same argument can be made regarding PSP-measured solar flux. The ice crystals found in mixed-phase stratus clouds tend to be an order of magnitude larger in size than typical water droplets with much lower concentrations. Consequently, compared to water droplets, the large ice crystals lead to more forward scattering that may compensate the direct solar transmission loss attenuated by the ice particles. This argument becomes more reasonable when the solar transmission is totally dominated by the diffuse component under optically thick conditions. Therefore, it is reasonable to assume that it is possible to apply the D97 approach to certain mixed phase clouds.

Advanced Very High Resolution Radiometer (AVHRR) data the NOAA-12 and 14 satellites were collected during FIRE ACE for an area centered on the SHEBA ship. The data consist of 1-km 0.65, 0.87, 3.75, 10.8, and 12.0-μm radiances. These datasets and their calibrations are described by *Minnis et al.* [2000], and TOA shortwave albedos

were also computed from the AVHRR 0.65-μm data [*Minnis et al.,* 2000; *Doelling et al.,* 2000] for a 25-km radius circle around the SHEBA ship. Near-nadir viewing Along-Track Scanning Radiometer (ATSR-2) [*Mutlow et al.,* 1999] data were also collected. The ATSR-2 carries a 1-km scanner with 0.65, 1.64, 3.75, 10.8, and 12.0-μm channels that makes a 512 x 570-pixel image.

The AVHRR data are analyzed with the Visible-Infrared-Solar infrared Technique (VIST) of *Minnis et al.* [1995] to obtain r_e and τ for a 20 x 20 km region centered at the SHEBA ship or the closest observable location near the ship. That technique matches the 0.65, 3.75, and 10.8-μm data with model calculations to derive the cloud properties and cloud-top temperature. Because the model parameterization can yield large optical depth errors when surface albedo exceeds 30% at 0.65 μm [*Minnis et al.,* 1993], a variation of the parameterization was developed to account for bright surfaces. This was accomplished by directly computing the TOA bidirectional reflectances for the combined surface, atmosphere, and cloud for each 0.05 increment of surface albedo between 0.35 and 0.90 using all of the cloud droplets and optical properties employed in the original parameterization [*Minnis et al.,* 1998]. This approach is termed the "bright surface model" of VIST (VISTB).

The ATSR-2 data were also analyzed with the original parameterization and a technique using the approach of *Platnick et al.* [1999, 2000]. The latter method termed the Near-Infrared-Solar infrared Technique (NIST) avoids the problems of the bright surface albedo at 0.65 μm by deriving optical depth from the 1.6-μm reflectance, because the albedos of snow, ice, and water are very small at this wavelength. The 3.75-μm radiance is used to derive the cloud droplet size in the same manner used in the VIST. To effect the retrieval, a set of cloud 1.6-μm reflectance models was developed to match those reported by *Minnis et al.* [1998].

Four research aircraft were deployed during FIRE ACE. Only data from the National Center for Atmospheric Research (NCAR) C-130Q are available for this study.

The Forward Scattering Spectrometer Probe (FSSP-100) on the C-130Q research aircraft provided in situ measurements of the cloud microphysical properties. The FSSP-derived cloud-droplet effective radius and number concentration are used and agree very well with Gerber Scientific Particulate Volumn Monitor (PVM-100A) measured cloud droplet size in three cases. There are discrepancies in cloud liquid water contents LWC between FSSP, PVM, and the King hot-wire measurements [*Lawson et al.,* 2000], and further study is needed. Therefore, the aircraft-measured cloud liquid water contents are not used for comparison with surface measurements in this study.

3. Cloud properties

We use three cloudy cases (May 4/5, 15/16, and 27/28) to represent the transition regime of Arctic stratus clouds. A mixed phase stratus event occurred on May 4/5 (T_{cldy} $\sim$ -22 C; Case 1). The cloud system over the SHEBA ship was predominately liquid phase on May 15/16 (T_{cldy} $\sim$ -8 C; Case 2) while on May 27/28 the cloud was liquid phase only (T_{cldy} $\sim$ 1 C; Case 3). The NCAR C-130Q aircraft and AVHRR and ATSR-2 data are also available for these three cases. Vertical profiles of temperature and relative humidity measured by radiosondes for the three cloudy days are shown in Figure 1. The surface temperatures of three case days increased from -15 C of Case 1, to -5 C of Case 2, to 1 C of Case 3 (Figure 1).

a. Case 1, May 4/5

The cloud properties of Case 1 are more complicated than the other two cases because the mixed phase cloud layer (Figure 2) occurred between two ice crystal layers as shown in radar and lidar images (see Figure 2 of *Curry et al.,* 2000). The ice crystals from the dissipating altostratus cloud fell through the mixed phase cloud layer to the surface. As shown in Figure 2, the ceilometer-measured cloud base height is around 0.6 km. Because the radar-derived cloud top height is near the top of the ice crystal layer ($\sim$ 4 km), we used visual inspection of the radar reflectivity and Doppler spectrum

gradients, and radiosonde sounding to set the cloud top of the mixed phase layer at 1.1 km. The fixed cloud-top height only affects the retrieved N. In the layer between the ceilometer-detected cloud base and 1.1 km, there is about equal amounts of ice and liquid (see Figure 3 of *Curry et al.,* 2000). The ice particles determined from the Cloud Particle Imager (CPI) show a monotonic decrease from cloud top to cloud base with a concentration about 200 L^{-1}. The ice particle size can be as small as water droplets near cloud top and as large as 1 mm near cloud base [*Curry et al.,* 2000; *Lawson et al.,* 2000]. The CPI-determined water droplets have the same values and vertical variations as the FSSP measurements. In general, the ratio of water droplet to ice particle concentration is greater than 1000:1 [*Lawson et al.,* 2000]. Therefore, water droplets dominate the microphysical and radiative properties of this mixed-phase cloud layer.

The aircraft data were also averaged to a 5-min temporal resolution when the aircraft is within a radius of 10 km of the SHEBA ship. The vertical location of the aircraft relative to the cloud boundaries is illustrated in Figure 2. The aircraft systematically sampled from the top to the bottom of the cloud layer resulting in the expected linear decrease of FSSP-derived r_e. Since the D97 approach generates an extinction-weighted mean value of r_e, we expect the comparison with the aircraft-measured values to be best in the middle to upper portions of the layer where the conjunction of the higher liquid water contents and larger droplets occur [*Dong et al.,* 1998; *Mace and Sassen,* 2000]. Given the large sampling difference between the aircraft (0.016 m^3) and surface (10^7 m^3) in 5-min intervals [*Dong et al.,* 1998], as well as the uncertainties in the in situ data and the retrievals, the effective radius comparison is about as good as we could expect.

The concentration comparison shows substantial disagreement between the surface and in situ data. The high values of N relative to the combined surface instrument retrievals may be due to (1) the result of small ice crystals affecting the FSSP data, (2) uncertainties in the surface estimated cloud thickness, (3) uncertainties in microwave-radiometer-derived LWP, and (4) the assumption of constant droplet size

distribution. From FSSP data, the mean logarithmic width is about 0.29 with the range of 0.2 to 0.7. If the FSSP-estimated droplet size distribution were introduced into the surface retrieval, it would make the comparison worse and further complicate the matter. Also, the FSSP estimates of the droplet size distribution may not be very reliable in such a complicated cloud condition or if the cloud droplet dsitribution is bimodal. *Dong et al.* [1997] have shown that the retrieved N is very sensitive to cloud LWP, droplet size distribution and cloud thickness. For example, the retrieved N can increase up to 30% if the logarithmic width increases from 0.35 to 0.5, to 25% if the cloud cloud thickness drops from 500 m to 400 m, and to 50% if the cloud LWP decreases about 20%.

For the surface retrieval, the D97 approach should work well for mixed phase clouds when the ice particles are much larger and substantially fewer than water droplets as we discussed in section 2. However, the small ice particles in this case may decrease the solar transmission and result in an overestimation of N and underestimation of r_e. If we estimate ice water path and mean ice crystal effective radius from Figures 3 and 4 of *Curry et al.* [2000], they are about 30 $\mathrm{g\,m^{-2}}$ and 75 μm. Consequently, the cloud optical depth induced by ice particles is less than 1, a value that is much smaller than those in Figure 2 and that has minimal impact on the solar flux measurements. Therefore, the D97 approach should work well for this case. The agreement between the surface, satellite, and aircraft results for r_e suggest that the optical depth is correct from the surface. As shown later, the computed radiative flux supports this conclusion.

The VIST retrievals of NOAA-14 AVHRR data taken at 2121 UT 4 May 1998 produced $r_e = 9.5$ μm and $\tau = 56$ for T_c= 248 K. Applying the VISTB with a clear-sky reflectance of 0.72 gave the same values for T_c and r_e, but $\tau = 26.7$. The cloud temperature corresponds to an altitude of 1 km which is the level of the inversion base (Figure 1). Thus, it is likely that the overlying ice crystal cloud had an inconsequential optical depth. The VIST retrieval of τ is unrealistic for this case. The parameterization

does not allow cloud reflectance to be less than the clear-sky reflectance which is the case here. The VISTB value may be closer to the true quantity but it is difficult to discern here. Satellite retrievals using the 1.6-μm channel may help resolve the optical depth uncertainties.

There were no ATSR-2 data taken directly over the ship. However, from a satellite perspective, the cloud deck was uniform over a large area [*Curry et al.,* 2000]. Thus, it should be possible to use a comparison of AVHRR and ATSR-2 from a nearby area to infer what the ATSR-2 retrievals would yield over the SHEBA ship. For a 10 x 10 pixel box centered 175 km northeast of the ship, the VIST produced $r_e = 8.5$ μm, $\tau = 54.5$, and $T_c = 248$ K using the ATSR-2 data taken at nearly the same time. Similarly, the VIST derived a value of $r_e = 9.5$ μm, $\tau = 57$, and $T_c = 248$ K from collocated AVHRR data. VISTB produced $r_e = 9.5$ μm, and $\tau = 32.5$. These AVHRR results are very similar to the retrievals taken directly over the SHEBA ship. The NIST, which uses the 1.6-μm channel for optical depth yields $r_e = 11.1$ μm and $\tau = 8.5$. Because the 1.6-μm channel gives much better contrast between the snow and the clouds, it is expected than it would produce a more accurate value of optical depth over snow that can be determined from the visible channel. Because of the similar AVHRR radiances and retrievals over the SHEBA ship, it can be concluded that the cloud is extremely homogeneous and the ATSR-2 retrieval 175 km away is similar to what would be expected over the ship. Thus, the satellite retrievals yield effective droplet sizes that are well within the range retrieved from surface data and observed from aircraft. Similarly, the apparently more reliable retrieval from the ATSR-2 NIST suggests that the surfaced-based optical depth retrieval is closer to the true value in this case.

b. Case 2, May 15/16

The comparison of in situ-observed cloud microphysics and those calculated from the surface data show good agreement in Case 2 (Figure 3). However, the field is considerably variable and other data are needed to compare with the surface retrievals

during the time period without aircraft data. NOAA-14 AVHRR data taken at 0022 UT May 16 were analyzed with the VISTB to determine r_e and τ for the area around the ship. The r_e varied between 14 and 24 μm with a mean value of 20 μm. The values of r_e from the surface retrieval vary from 8 to 24 μm for the hour centered on the satellite overpass with a mean value of 15.3. The surface-retrieved τ is between 4 and 10, much less than the VISTB result. Use of the surface-derived τ would reduce the VISTB r_e by 1-2 μm. Although the surface-derived r_e value is less than that derived from the satellite data, the range is similar and the difference can be explained by the differences in τ. While a NIST retrieval is desirable to obtain a more accurate optical depth, no ATSR-2 data were taken near the ship that day.

c. Case 3, May 27/28

In Case 3, the surface-retrieved r_e is twice as large as the aircraft value as shown in Figure 4. The variability of the surface retrievals and the great difference in r_e between the aircraft and the surface suggests that the two platforms may have sampled different cloud regimes. For instance, Figure 4 shows that the aircraft was sampling above the radar-derived cloud top between 2235 and 2245 UT and below the ceilometer-measured cloud base between 2345 and 2415 UT.

Satellite imagery also suggests strong horizontal gradients as the cloud moves over the region. The 3.75-μm image from the NOAA-14 overpass at 2349 UT, 27 May 1998 in Figure 5 shows two distinct cloud types in the vicinity of the ship (The ship was located at the center of the box in the figure). The brightness temperatures from the 10.8-μm channel vary by 1-2 K indicating that the cloud-top heights are somewhat variable. However, this variability on cloud-top height does not account for the variabilities seen in the 3.75-μm image. The brightness temperature differences between the 3.75 and 10.8-μm channels in the box range from 8 K to 35 K, an indication of substantial variations in droplet size.

The mean value of r_e from VISTB is 13.5 μm with T_c = 250 K (0.4 km) and

$\tau = 37.4$. The mean value of r_e belies the structure of the clouds seen in the imagery, however. The histogram of retrieved droplet sizes in Figure 6 show an almost bimodal distribution confirming two distinct cloud types in the vicinity of the ship. One has a peak around 10.5 μm, while the other maximizes at 20 μm. Because the VISTB finds these clouds to be optically thick, it is assumed that the 3.75-μm reflectance has reached its maximum value for both cloud types.

Again, there are no ATSR-2 data taken directly over the ship; its location was between two adjacent nadir view ATSR-2 images at 2347 UT. Just to the north of the camp, the NIST retrieval yields $r_e = 8.6$ μm and $\tau = 7.4$, while in the adjacent image just to the south of the ship, the NIST derives $r_e = 21.6$ μm and $\tau = 10.4$. The latter are more like the surface retrieval, while the former are extremely close to the aircraft results. Thus, it can be concluded that the surface and aircraft were observing two different clouds, which has been verified in Figure 7 where the aircraft flew mostly over the north of the ship. The values of r_e from AVHRR VISTB retrieval over the small droplet cloud are 2 μm greater than the NIST retrieval. This difference is due to the differences in the retrieved optical depths. If τ is assumed to be 7.4 for the VISTB retrieval, then the NIST and AVHRR values of r_e would coincide.

d. Discussion:

Although these comparisons using the surface, aircraft, and satellite data are quite limited, it appears that both the VIST and VISTB can yield reasonably accurate values of cloud effective particle size if the cloud is optically thick. Both techniques overestimate τ, so it will be difficult for them to differentiate optically thick and thin clouds. The NIST appears to be a very promising method for accurately retrieving both particle size and optical depth over snow and ice which are highly reflective at visible wavelengths. It may also be possible to use infrared methods to derive cloud optical properties for thin clouds over the snow, but the clouds need to show sufficient temperature differences between the 10.8 and 12-μm channels to effect a retrieval. Such

differences were not seen in the data examined here. Additional study is needed to determine if infrared methods will be applicable to a significant population of Arctic clouds.

The surface-based retrievals agree reasonably well with the aircraft measurements, but it is clear that the two systems must be viewing the same clouds to effect meaningful comparisons. Although the clouds appear to be extremely uniform, the May 4 case may be affected by the ice crystals in the stratus. The surface retrieval assumes the cloud is only composed of liquid water while the ice crystals may contribute to the aircraft measurements. Thus, it is difficult to draw any quantitative conclusions from this case.

The clouds were highly variable during Cases 2 and 3. LWP varied by a factor of two during the aircraft flights on both days. And it has been demonstrated that the aircraft and surface were, for the most part, sampling two completely different clouds in Case 3 because the boundary of the two clouds was very close to the ship [Figure 5]. The sudden spike in N and dip in r_e from the retrieval at 2250 UT [Figure 4] suggest that the cloud boundary passed over the ship at that time. Despite the difficulties, both the aircraft and surface retrievals seem to be very reasonable when the variability observed from the satellite is considered. While it may be concluded that the satellite and surface retrievals are certainly very reasonable, much more data are need to make a reliable quantitative assessment of the accuracy of either remote sensing approach.

Dong et al. [1998] have discussed the comparison of aircraft in-situ measurements and surface retrievals with D97 approach, and concluded that since the layer-mean cloud parameters derived from the D97 scheme are weighted by the extinction profile of the layer, the aircraft validation should be derived primarily from the upper 1/3 of the layer. *Dong et al.* [1998] also show that the aircraft-derived values of r_e generally increase with height while N remains approximately constant, as seen in many previous aircraft studies. The FSSP-derived values of r_e in Case 1 are similar to *Dong et al.* [1998] and other studies, while those in Cases 2 and 3 are quite different from previous

studies. For example, the cloud droplets near cloud top are *smaller* than at cloud base (2200 UT, Figure 3), while there is no systematic variation in cloud droplets with height when aircraft samples from cloud top to cloud base during a 1.5 hour time period (Figure 4). It is obvious that not all Arctic stratus clouds follow the accepted conceptual model of middle latitude continential and marine stratus clouds. Based on the retrievals from radar and microwave radiometer measurements, *Shupa et al.* [2000] have found that cloud droplet size and liquid water content for the Arctic increase from cloud base through about the lowest 1/3 of the cloud layer, then decrease up to cloud top. We performed additional analyses of the Case 2 data and reached the same conclusion. A full understanding of the variability of Arctic stratus cloud properties is beyond our current knowledge, and more studies are needed.

Recent comparisons of the aircraft and surface radiometer retrievals suggest that the LWP derived from the surface microwave radiometer may be overestimated by about 15-20% [J. Curry, personal communication, 2000]. If it is true, then the surface-retrieved r_e will decrease and N will increase resulting in better agreement between the surface and aircraft values for Cases 1 and 2. The exact change in microwave-radiometer-derived LWP will need to be determined for each case to quantify the change in the surface retrievals of r_e and N. Such an analysis will be undertaken when the uncertainties in the microwave-radiometer-derived LWP are resolved.

4. Radiation budget

According to model simulations [*Curry et al.,* 1996] and analysis of satellite data [*Rossow and Zhang,* 1995], Arctic stratus clouds have a net warming effect on the surface during the winter and a net cooling effect on the surface during the summer. During the winter season, there is no solar energy, and since snow radiates nearly as a blackbody, the surface cools substantially. Arctic stratus clouds tend to trap the surface-emitted thermal infrared radiation that would normally escape to space. The

stratus then act as a heat source by radiating energy back to the surface leading to a net warming effect. This heating effect is particularly true in cases where the stratus exist in strong temperature inversions. During the summer season, much of the highly reflective snow surface has been melted and solar energy can be absorbed by the low albedo surface during the long Arctic day. Arctic stratus clouds, with their high albedo, can reflect a substantial fraction of this incident solar energy back to space leading to a net cooling of the surface over what would occur under clear skies. During the spring transition season, it is difficult to ascertain the sign of the cloud feedback to the surface because the melting of ice may result in an abrupt change in the surface albedo that can trigger a whole family of coupled and very nonlinear feedback mechanisms [*Stamnes et al.,* 1999]. To address this question, the surface radiative forcing is studied here using precision radiometer-measured fluxes.

The model-calculated cloud albedos in Figures 8, 9, and 10 are nearly the same as the surface albedos. The combination of a highly reflective cloud over a highly reflective surface should produce a greater total albedo than either the cloud or the surface alone. The results of *Doelling et al.* [2000] based on AVHRR data show that the TOA albedo is at least 0.05 greater than the clear-sky albedo during May over the SHEBA area. The TOA albedos from AVHRR agree well (instantaneous uncertainty in the AVHRR results is +/- 0.04) with the surface-derived values in Case 1 (Figure 8) indicating that perhaps the surface-derived particle sizes and optical depths may be correct in this instance. However, the TOA albedos derived with the surface-retrieved cloud properties during Case 2 (Figure 9) are almost 0.05 less on average than AVHRR-derived values. This discrepancy is likely due to the variable cloud or due to uncertainties in radiative transfer model calculations. The surface-derived TOA albedos computed for Case 3 (Figure 10) are 0.08 less than the satellite-based value. In this case, the optical depths from the satellite and surface are in good agreement, but the droplet sizes vary. As shown by *Dong et al.* [1998], the computed cloud albedo increases by approximately 0.10 when

r_e changes from 12 to 20 μm for a constant LWP. Thus, since the cloud microphysics retrieved by the satellite are dominated by smaller droplets, the TOA albedo should be significantly greater than that computed for the value of r_e derived from the surface site. These cases show some interesting differences that may be explained by retrieval errors or spatial differences. Closer examination of the data and a study of the uncertainties in the surface instrumentation are needed. It is clear, however, that determination of the cloud radiative forcing at the TOA from surface-based data in the Arctic may not be reliable. While not much effect is computed from the surface, the satellite data indicate a net cloud forcing of -16 $\mathrm{W\,m^{-2}}$ for the atmosphere-earth system.

Conversely, the surface datasets are best for determining the cloud forcing at the surface. The net flux at the surface varies from 56 $\mathrm{W\,m^{-2}}$ on May 4 to 118 $\mathrm{W\,m^{-2}}$ on May 27. This significant increase in net flux is partially due to a decreasing solar zenith angle, surface albedo, and cloud optical depth. Data taken during May 23-25 (Figures 11 and 12) show a net flux of $\sim$ 97 $\mathrm{W\,m^{-2}}$ which is $\sim$ 20 $\mathrm{W\,m^{-2}}$ less than found for May 27. If it is assumed that the clear-sky conditions during May 23-25 are the same as they would be May 27, it may be concluded that the clouds caused a net heating of the surface. Thus, they would be producing a net cooling of the atmosphere because of the negative cloud forcing at the TOA. If the differences in surface albedo between May 4 and May 24 are taken into account and it is assumed that the clear-sky longwave properties are the same, the clouds would produce net forcings at the surface of 11 and 23 $\mathrm{W\,m^{-2}}$ during May 4/5 and May 15/16, respectively. These values are greater than that predicted using ISCCP data [*Curry et al.,* 1996] but much less than the net surface forcing estimated by *Curry and Ebert* [1992]. However, this study only considers stratus clouds. Stratus is the predominant cloud type during this period, but the inclusion of other cloud types would alter the conclusions to some extent.

The extra net flux at the surface due to the clouds would accelerate the melting of the ice. Rising surface and air temperatures are more directly related to the

increasing water vapor mixing ratio, therefore enhancing cloud formation. The process is dominated by the availability of the additional infrared flux because the clouds are often warmer than the surface. As the inversion structure changes during the summer, this net cloud forcing effect may not hold. Furthermore, as the surface albedo decreases with the onset of summer, the cloud albedo will become more important because of increased contrast between the surface and the cloud. Thus, it will be necessary to perform additional case studies throughout the FIRE ACE period using both surface and satellite data to determine the variation in the effects of clouds on the Arctic surface energy budget.

5. Concluding Remarks

Arctic stratus cloud macrophysical, microphysical, and radiative properties during the spring transition season were examined using a variety of platforms and sensors. The mean cloud droplet effective radii varied from 8 to 20 μm, while optical depths ranged from 5 to 22 depending on the platform and excluding visible-channel satellite retrievals. The surface-based data yielded mean optical depths between 5 and 12. In all of the considered cases, either the surface-derived effective particle sizes or number concentrations agreed with the corresponding in situ data, but not both at the same time. While it is possible that the discrepancies may be due to instrumental or algorithmic uncertainties, they can also arise from the effects of ice crystals in otherwise liquid clouds; mismatches between the aircraft and surface in a highly variable cloud field; and cloud vertical structure that is not totally sampled by the aircraft measurements. Thus, even in stratus clouds, validation of surface-based retrievals can be a difficult process. Certainly, examination of the instrumental errors and impact of ice crystals on the algorithms is warranted. Analyses of additional cases later in the experiment may also shed some additional light on the differences seen here.

Satellite data proved critical for understanding some of the observed discrepancies

despite ambiguities in the retrievals. The satellite-derived particle sizes agree well with the coincident surface retrievals. Matches with the satellite data were not obtained in these cases, although later flights during FIRE ACE may yield better coincidence between satellite and aircraft measurements in the clouds. Optical depths derived from visible-channel data over snow backgrounds appear to be overestimated in all three cases. The derived cloud optical depth is very sensitive to the surface albedo specified for the retrieval and can be easily overestimated. This result suggests that methods currently using the visible channel to derive cloud optical depth may overestimate it in polar regions. Although not available on most current satellites, it appears that a near-infrared channel with a solar infrared channel may alleviate this overestimation problem. Instruments with 1.6-μm channels like that on the ATSR-2 are being flown more often and should provide better coverage of the poles. While the initial 1.6-μm results are encouraging, they are not totally conclusive and further study of the satellite-derived cloud optical depths near the poles is needed. The combination of radar and radiometer data at the SHEBA site has proven invaluable for elucidating the uncertainties of the optical depth retrieval and will be required to reliably quantify the errors in the satellite retrievals. This need highlights the importance of resolving the surface and in situ retrievals.

It appears that, overall, Arctic stratus clouds have a warming effect on the surface for the May transition period, roughly 20 $\mathrm{W\,m^{-2}}$ net flux at the surface compared to the clear-sky condition. This extra energy should accelerate the melting of snow/ice surface and provide additional moisture to the boundary layer for cloud formation. Conversely, the satellite data show that the clouds have a net cooling effect on the system during May suggesting that the atmosphere above the clouds is cooling relative to the clear-sky condition. Such an effect would reinforce the subsidence and help maintain the boundary layer inversions despite the increased energy at the surface. The availability of more moisture in the boundary layer would help maintain the Arctic

stratus. As the ice pack melts, however, the stratus cloud warming would likely change to a cooling effect at the surface because the relative amount of solar energy available for absorption will be significantly reduced.

This study has focused on only three cloud cases during May and has clearly shown their radiative effect during the transition period. Although stratus clouds are predominant in the summertime Arctic, other types of clouds occurred that affect the radiation budget differently. Thus, an analysis of SHEBA and FIRE ACE datasets is needed to fully understand the role of clouds during the annual melting and refreezing process that occurs in the Arctic. The results in this paper provide an important part of that analysis process.

Acknowledgments. The authors would like to thank two anonymous reviewers for their insightful suggestion of this work. The surface-based data were obtained from the Atmospheric Radiation Measurement (ARM) Program sponsored by the US Department of Energy (DOE), Office of Energy Research, Office of Health and Environmental Research, Environmental Sciences Division. The aircraft data were provided by the NCAR C-130Q staff and scientists that participated in the FIRE experiment, and special thanks to Mr. Ron Ruth, the data manager, to provide the aircraft data promptly that makes this comparison available. The radar data were provided by Taneil Uttal. The ATSR-2 data were made available by Rutherford Appleton Laboratories, Chilton, Didcot, Oxfordshire, UK. Bob Arduini and Jessica Woods-Vedeler provided assistance with the satellite algorithm development. During this study, Xiquan Dong and Gerald G. Mace were supported by the ARM Program under Grant DE-AI02-97ER62341, NASA CERES program under contract NAG-1-2250, and NASA EOS validation program under contract NAG-5-6458. Pattrick Minnis and David F. Young were supported by NASA Earth Sciences Enterprise FIRE Program under the Radiation Division and by the Environmental Sciences Division of the U.S. Department of Energy Interagency Agreement DE-AI02-97ER62341 as part of the ARM Program.

References

Boers, R., Simultaneous retrievals of cloud optical depth and droplet concentration from solar irradiance and microwave liquid water path. *J. Geophys. Res., 102,* 29,881-29,891, 1997.

Curry, J. A. and E. E. Ebert, Annual cycle of the radiation fluxes over the Arctic Ocean: Sensitivity to cloud optical properties. *J. Climate, 5,* 1267-1280, 1992.

Curry, A.C., W.B. Rossow, D. Randall, and J.L. Schramm, Overview of arctic cloud and radiation characteristics. *J. clim., 9,* 1731-1764, 1996.

Curry, J.A., et al., FIRE Arctic Clouds Experiment. *Bull. Am. Meteorol. Soc.,* 81, 5-29, 2000.

Doelling, D.R., P. Minnis, C. Venkatesan, A. Mahesh, F.P.J. Valero, and S. Pope, Cloud radiative forcing during FIRE ACE derived from AVHRR data. Accepted by *J. Geophys. Res.,* this issue, 2000.

Dong, X., T.P. Ackerman, E.E. Clothiaux, P. Pilewskie, and Y. Han, Microphysical and radiative properties of stratiform clouds deduced from ground-based measurements. *J. Geophys. Res., 102,* 23,829-23,843, 1997.

Dong, X., T.P. Ackerman, and E.E. Clothiaux, Parameterizations of microphysical and shortwave radiative properties of boundary layer stratus from ground-based measurements. *J. Geophys. Res., 103,* 31,681-31,693, 1998.

Dong, X., P. Minnis, T.P. Ackerman, E.E. Clothiaux, G.G. Mace, C.N. Long, and J.C. Liljegren, A 25-month database of stratus cloud properties generated from ground-based measurements at the ARM SGP site. *J. Geophys. Res., 105,* 4529-4537, 2000.

Harrison, E.F., P. Minnis, B.R. Barkstrom, V. Ramanathan, R.D. Cess, and G.G. Gibson, Seasonal variation of cloud radiative forcing derived from the Earth Radiation Budget Experiment. *J. Geophys. Res., 95,* 18,687-18,703, 1990.

Hartmann, D.L., M.E. Ockert-bell, and M.L. Michelsen, The effect of cloud type on earth's energy balance: Global analysis. *J. clim., 5,* 1281-1304, 1992.

Kato, S., T.P. Ackerman, E.E. Clothiaux, J.H. Mather, G.G. Mace, M.L. Wesely, F. Murcray,

and J. Michalsky, Uncertainties in modeled and measured clear-sky surface shortwave irradiances. *J. Geophys. Res., 102,* 25,881-25,898, 1997.

Lawson, R.P., B.A. Baker, and C.G. Schmitt, Overview of microphysical properties of summertime boundary layer clouds observed during FIRE.ACE. Accepted by *J. Geophys. Res.,* this issue, 2000.

Lin, B., B. Wielicki, P. Minnis, and W. Rossow, Estimation of water cloud properties from satellite microwave, infrared and visible measurements in oceanic environments 1. Microwave brightness temperature simulations. *J. Geophys. Res., 103,* 3873-3886, 1998.

Mace, G.G., and K. Sassen, A constrained algorithm for retrieval of stratocumulus cloud properties using solar radiation, microwave radiometer, and millimeter cloud radar data. Accepted by *J. Geophys. Res.,* 2000.

Manabe, S., and R.T. Wetherald, Thermal equilibrium of the atmosphere with a given distribution of relative humidity. *J. Atmos. Sci., 24,* 241-259, 1967.

Minnis P., Y. Takano, and K.-N. Liou, Inference of cirrus cloud properties using satellite-observed visible and infrared radiances. Part I: Parameterization of radiance fields. *J. Atmos. Sci., 50,* 11279-1304, 1993.

Minnis, P., D.P. Kratz, J.A. Coakley, Jr., M.D. King, D.P. Garber, P.W. Heck, S. Mayor, W.L. Smith, Jr., D.F. Young, and R. Arduini, Cloud optical property retrieval (Subsystem 4.3). "Clouds and the Earth's Radiant Energy System (CERES) Algorithm Theoretical Basis Document, Volume III: Cloud Analyses and Radiance Inversions (Subsystem 4)", NASA RP 1376 Vol. 3, edited by CERES Science Team, December, 1995.

Minnis, P., D.P. Garber, D.F. Young, R.F. Arduini, and Y. Takano, Parameterization of reflectance and effective emittance for satellite remote sensing of cloud properties. *J. Atmos. Sci., 55,* 3313-3339, 1998.

Minnis, P., D. Doelling, C. Venkatesan, D.C. Spangenberg, L. Nguyen, R. Palikonda, T, Uttal, M. Shupe, and R.F. Arduini, Arctic cloud coverage during FIRE ACE derived from AVHRR data. Accepted by *J. Geophys. Res.,* this issue, 2000.

Mutlow, C.T., M.J. Murray, D.L. Smith, P.D. Watts, and P. North, New datasets for climate change and land use studies are on track. *Eos, 80,* 589-595, 1999.

Perovich, D.K., and coauthors, Year on ice gives climate insights. *EOS. Trans. Amer. Geophys. Union, 80,* 481, 1999.

Platnick, S., G.T. Arnold, M.D. King, S.-C. Tsay, H. Gerber, P.V. Hobbs, and A. Rangno, A technique for cloud retrievals over snow and ice surfaces with examples from FIRE-ACE. *Proc. AMS 10th Conf. Atmos. Rad.,* Madison, WI, 28 June - 2 July, 234-236, 1999.

Platnick, S., J.Y. Li, M.D. King, H. Gerber, and P.V. Hobbs, A solar reflectance method for retrieving cloud optical thickness and droplet size over snow and ice surfaces. Accepted by *J. Geophys. Res.,* this issue, 2000.

Ramanathan, V., R.D. Cess, E.F. Harrison, P. Minnis, B.R. Barkstrom, E. Ahmad, and D. Hartmann, Cloud-radiative forcing and climate: Results from the Earth Radiation Budget Experiment. *Science, 243,* 57-63, 1989.

Rossow, W.B., and Y.-C. Zhang, Calculation of surface and top-of-atmosphere radiative fluxes from physical quantities based on ISCCP datasets. Part II: Validation and first results. *J. Geophys. Res., 100,* 1167-1197, 1995.

Stamnes, K., R.G. Ellingson, J.A. Curry, J.E. Walsh, and B.D. Zak, Review of science issues, development strategy, and status for the ARM North Slope of Alaska-Adjacent Arctic Ocean climate research site. *J. clim., 12,* 46-63, 1999.

Stokes, G. M., and S. E. Schwartz, The Atmospheric Radiation Measurement (ARM) program: Programmatic background and design of the cloud and radiation testbed. *Bull. Am. Meteorol. Soc., 75,* 1201-1221, 1994.

Schneider, S.H., Cloudiness as a global climatic feedback mechanism: The effect on the radiation balance and surface temperature of variation in cloudiness. *J. Atmos. Sci., 29,* 1413-1423, 1972.

Young, D.F., P. Minnis, and R.F. Arduini, A comparison of cloud microphysical properties

derived using VIRS 3.7 and 1.6 μm data. *Proc. AMS 10th Conf. Atmos. Rad.,* Madison, WI, June 28 - July 2, 25-28, 1999.

X. Dong and G.G. Mace, Dep. of Meteorol., 819 Wm. C. Browning Bldg. University of Utah, Salt Lake City, UT 84112. (e-mail: xdong@met.utah.edu; mace@met.utah.edu)

P. Minnis, and D.F. Young, Mail Stop 420, NASA Langley Research Center, Hampton, VA 23681-0001.(e-mail: p.minnis@larc.nasa.gov; d.f.young@larc.nasa.gov)

Received ???, 1999; revised ???, 2000; accepted ???, 2000.

---

[1]Meteorology Department, University of Utah, Salt Lake City, Utah.

[2]NASA Langley Research Center, Hampton, Virginia.

To appear in the *Journal of Geophysical Research*, 2000.

Figure 1. Three cloudy soundings were launched around local noon (23 UT) from SHEBA ship at the locations of 76.013N/165.357W (May 04, Case 1), 76.297N/165.271W (May 15, Case 2), and 76.556N/168.004W (May 27, Case 3), respectively.

Figure 2. Cloud top height from the 35-GHz cloud radar (fixed at 1.1 km in this case), cloud base height from the laser ceilometer, and cloud liquid water path LWP from the microwave radiometer. The cloud-droplet effective radius r_e, number concentration N, and optical depth τ were retrieved from the δ2-stream model. The aircraft values of r_e and N were measured by the FSSP-100. Satellite results were retrieved from VISTB. 24 UT corresponds with 00 UT May 05.

Figure 3. Same as Figure 2 but for Case 2 and the cloud base height was fixed at 0.2 km based on the lidar image because the ceilometer measurement was not available on May 15.

Figure 4. Same as Figure 2 but for Case 3. The satellite results are shown in the north of the ship with N and the south of the ship with S.

Figure 5. The 3.75-μm (T3) and its temperature difference with 10.8-μm (T4) images from the NOAA-14 overpass at 2349 UT, 27 May 1998. The SHEBA ship is the center of the 20 x 20 km box.

Figure 6. The VISTB-retrieved r_e histogram shows that there are two distinct cloud types around the ship. The effective radii in the south of the ship are twice as large as those in the north of the ship.

Figure 7. NCAR C-130Q research aircraft flight patterns over the SHEBA ship during the May 27/28, 1998, Case 3.

Figure 8. The broadband downward/upward solar and infrared fluxes at the surface were measured by up-/down-looking standard Eppley precision spectral radiometers. The cloud and TOA albedos are derived from the δ2-stream model. Satellite-derived broadband TOA albedos are calculated from the empirical relationship between narrow band and broadband based on AVHRR-measured visible reflectance.

Figure 9. Same as Figure 8 but for Case 2.

Figure 10. Same as Figure 8 but for Case 3.

Figure 11. Same as Figure 8 but for clear-sky conditions. The modeled downward solar flux at the surface was calculated from the $\delta 2$-stream model with the input of measured surface albedo and sounding.

Figure 12. Same as Figure 11 but for another clear-sky day.

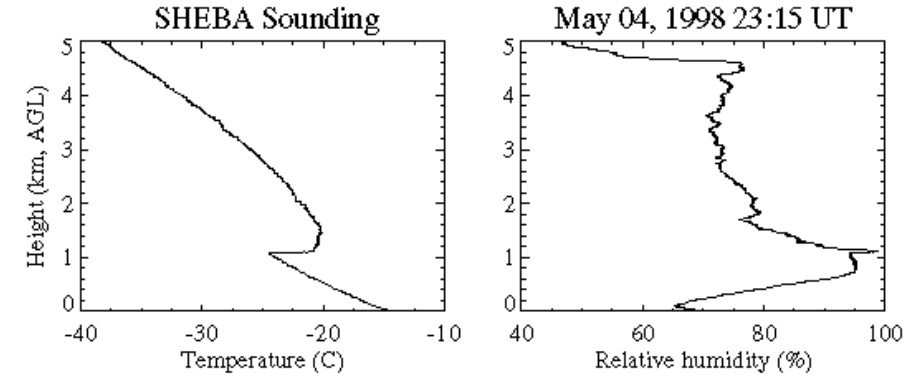
SHEBA Sounding
May 04, 1998 23:15 UT
Height (km, AGL)
Temperature (C)
Relative humidity (%)

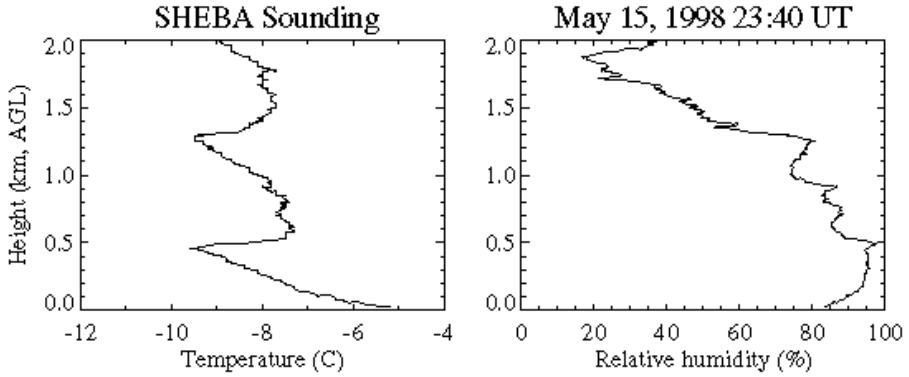
SHEBA Sounding
May 15, 1998 23:40 UT
Height (km, AGL)
Temperature (C)
Relative humidity (%)

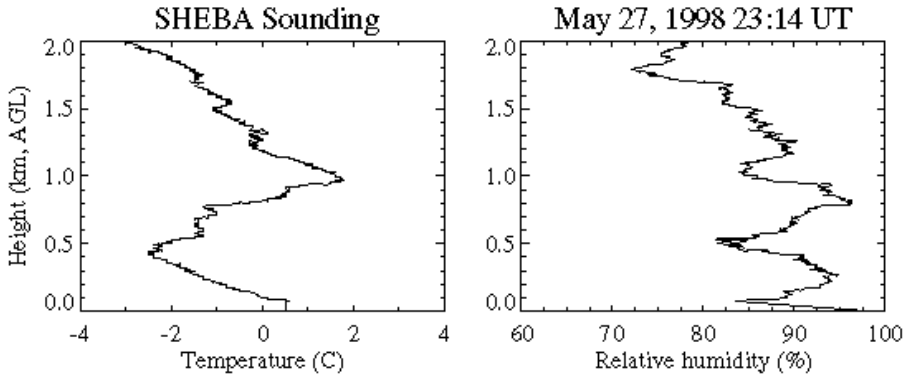
SHEBA Sounding
May 27, 1998 23:14 UT
Height (km, AGL)
Temperature (C)
Relative humidity (%)

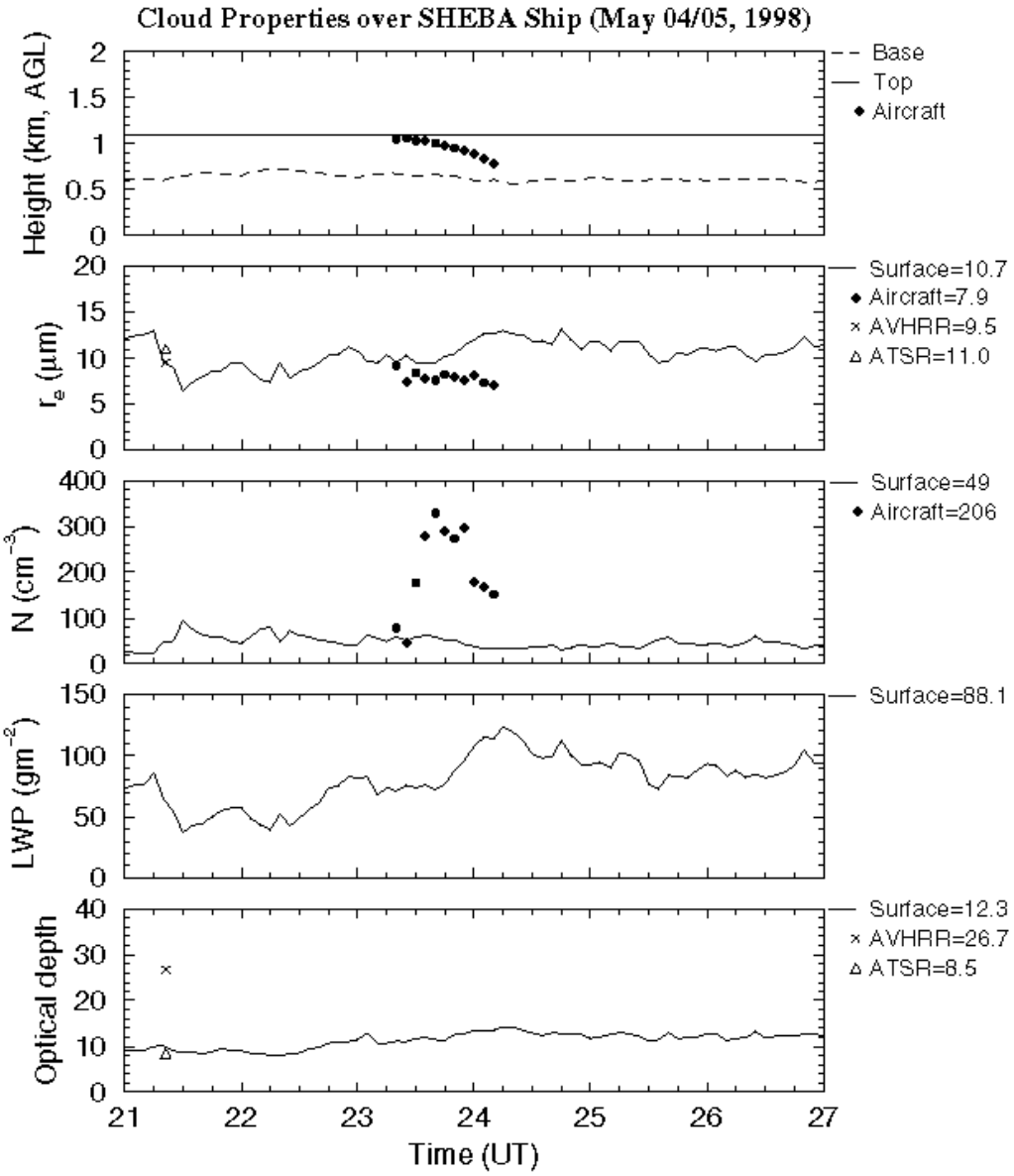
Cloud Properties over SHEBA Ship (May 04/05, 1998)
Height (km, AGL)
Base
Top
Aircraft
r_e (μm)
Surface=10.7
Aircraft=7.9
AVHRR=9.5
ATSR=11.0
N (cm^{-3})
Surface=49
Aircraft=206
LWP (gm^{-2})
Surface=88.1
Optical depth
Surface=12.3
AVHRR=26.7
ATSR=8.5
Time (UT)

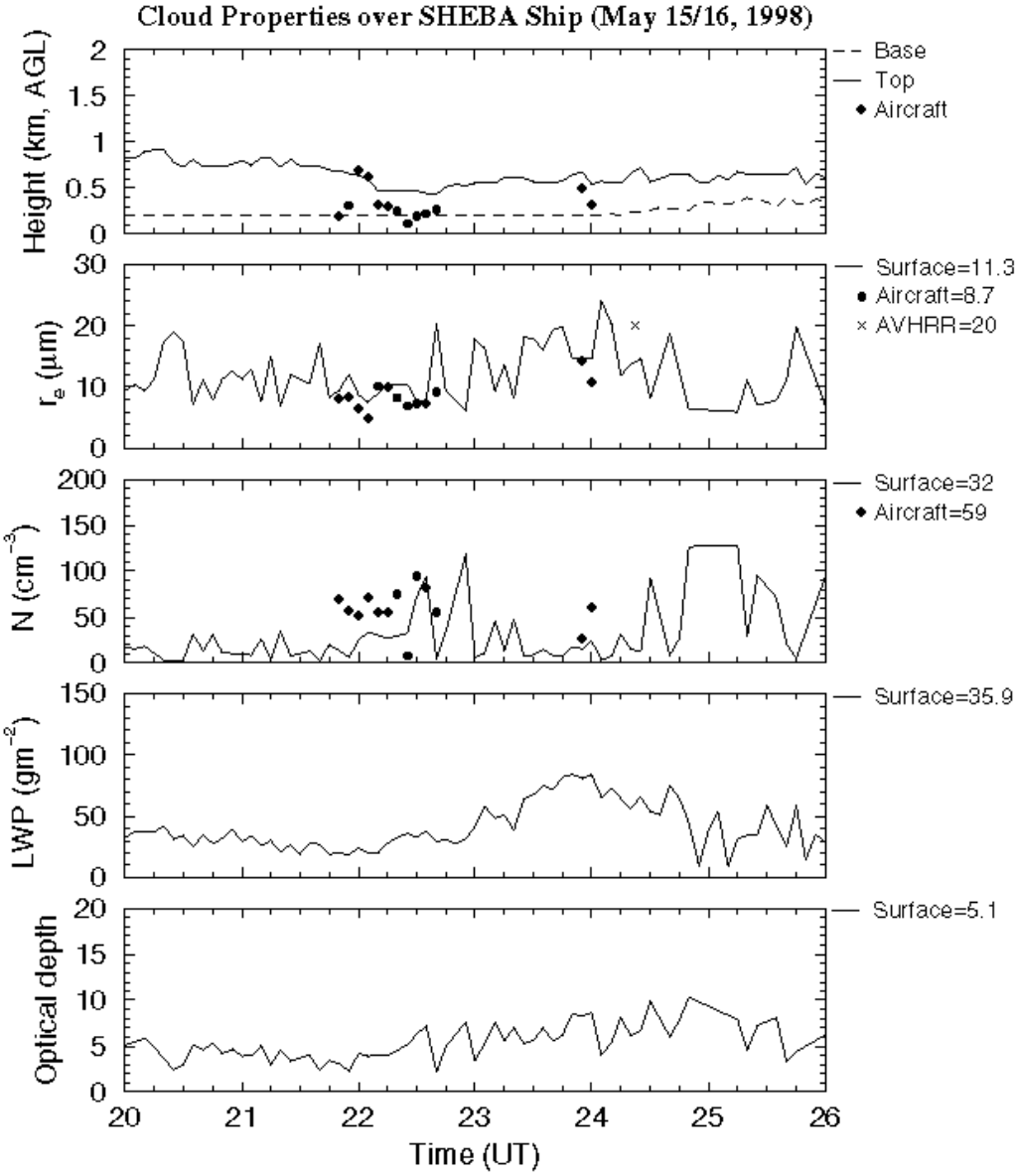
Cloud Properties over SHEBA Ship (May 15/16, 1998)
Height (km, AGL)
Base
Top
Aircraft
r_e (μm)
Surface=11.3
Aircraft=8.7
AVHRR=20
N (cm^{-3})
Surface=32
Aircraft=59
LWP (gm^{-2})
Surface=35.9
Optical depth
Surface=5.1
Time (UT)

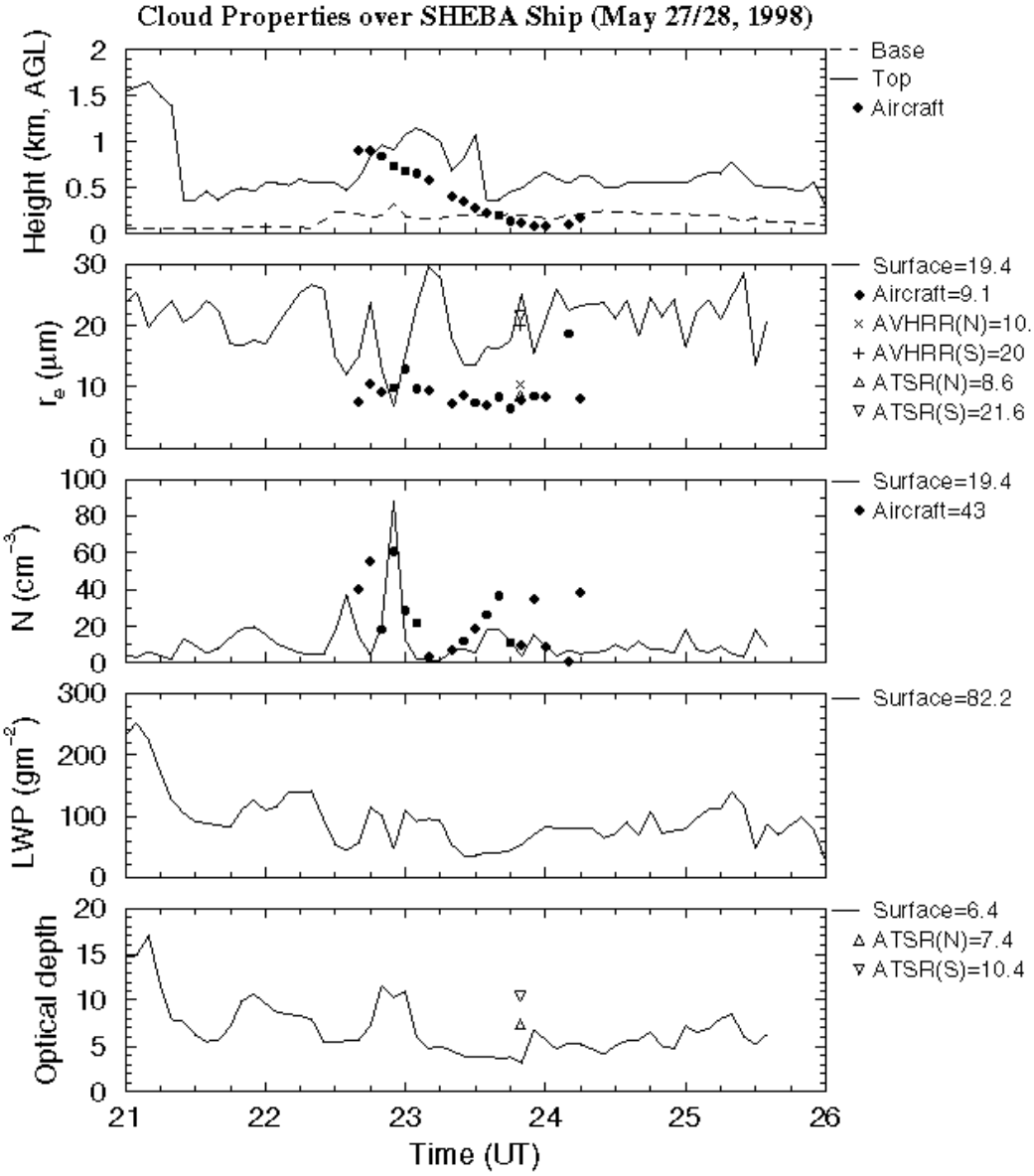
Cloud Properties over SHEBA Ship (May 27/28, 1998)
Height (km, AGL)
Base
Top
Aircraft
r_e (μm)
Surface=19.4
Aircraft=9.1
AVHRR(N)=10.5
AVHRR(S)=20
ATSR(N)=8.6
ATSR(S)=21.6
N (cm^{-3})
Surface=19.4
Aircraft=43
LWP (gm^{-2})
Surface=82.2
Optical depth
Surface=6.4
ATSR(N)=7.4
ATSR(S)=10.4
Time (UT)

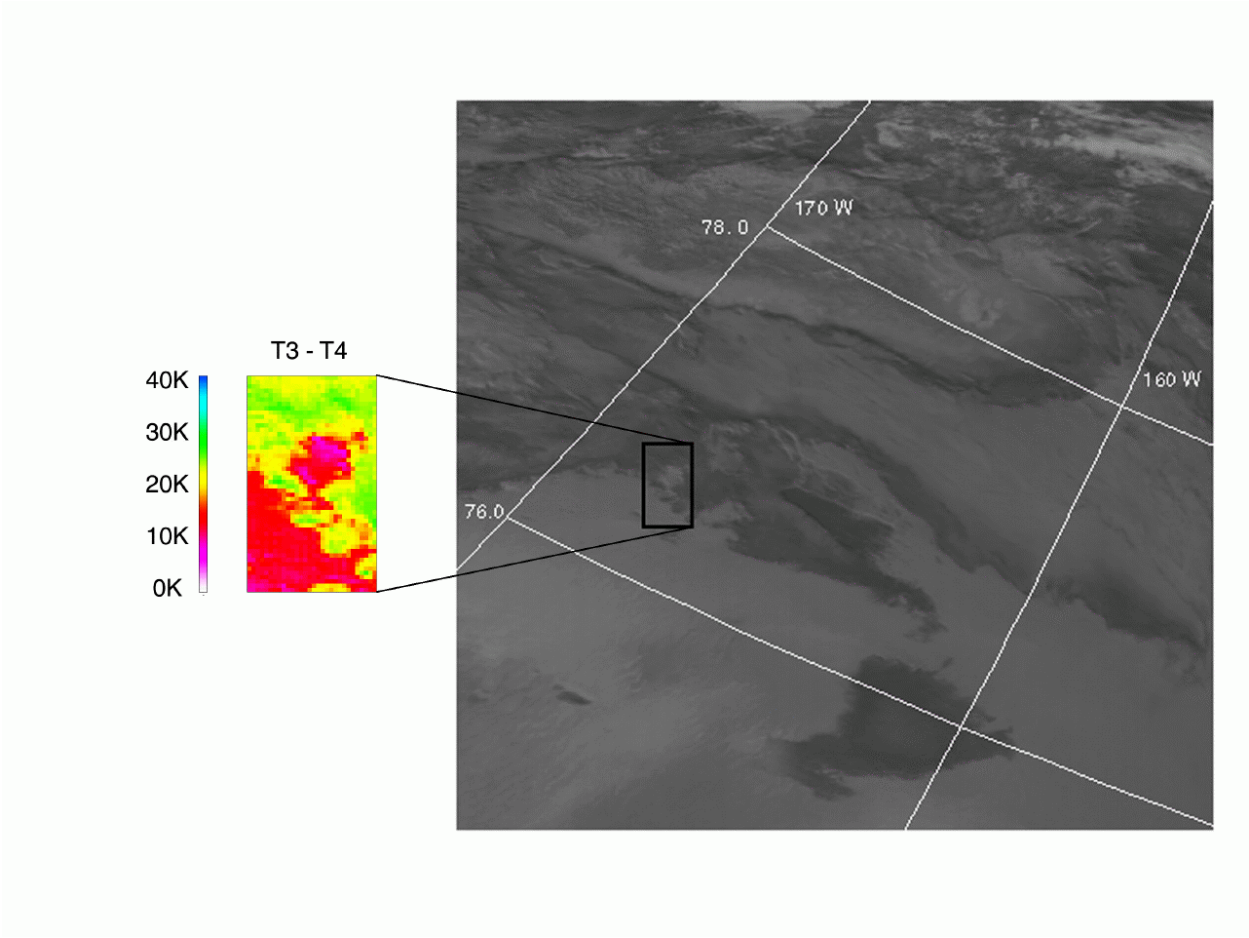
T3 - T4
40K
30K
20K
10K
0K
78.0
170 W
160 W
76.0

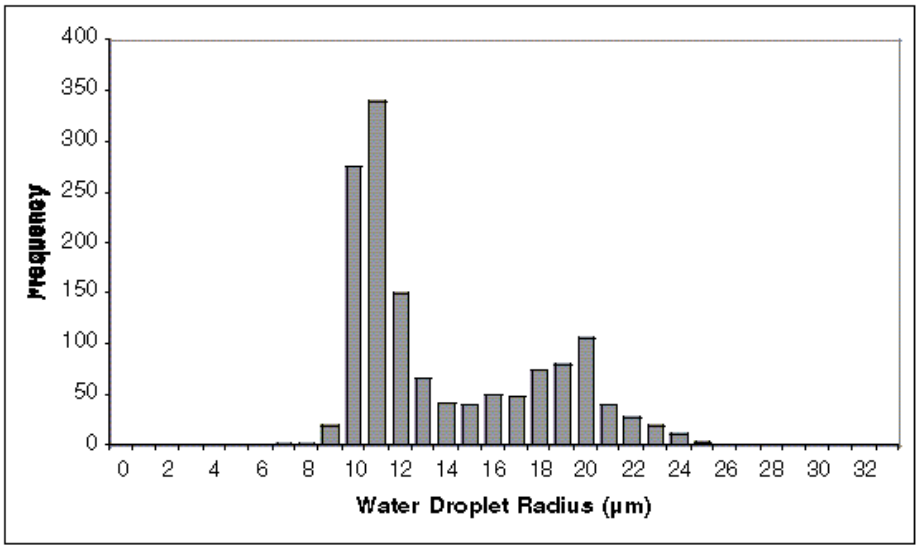
400
350
300
250
200
150
100
50
0
Frequency
0 2 4 6 8 10 12 14 16 18 20 22 24 26 28 30 32
Water Droplet Radius (µm)

Aircraft Flight Trajectory over SHEBA ship

Case 3 (2139 UT-->2417 UT, 5/27/98)

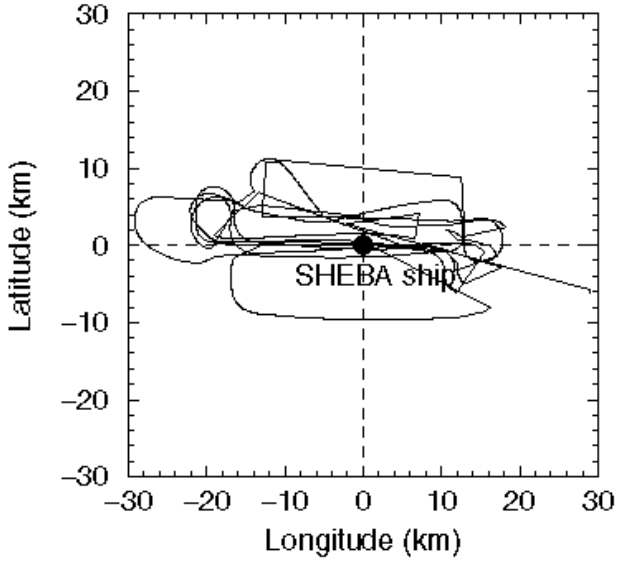

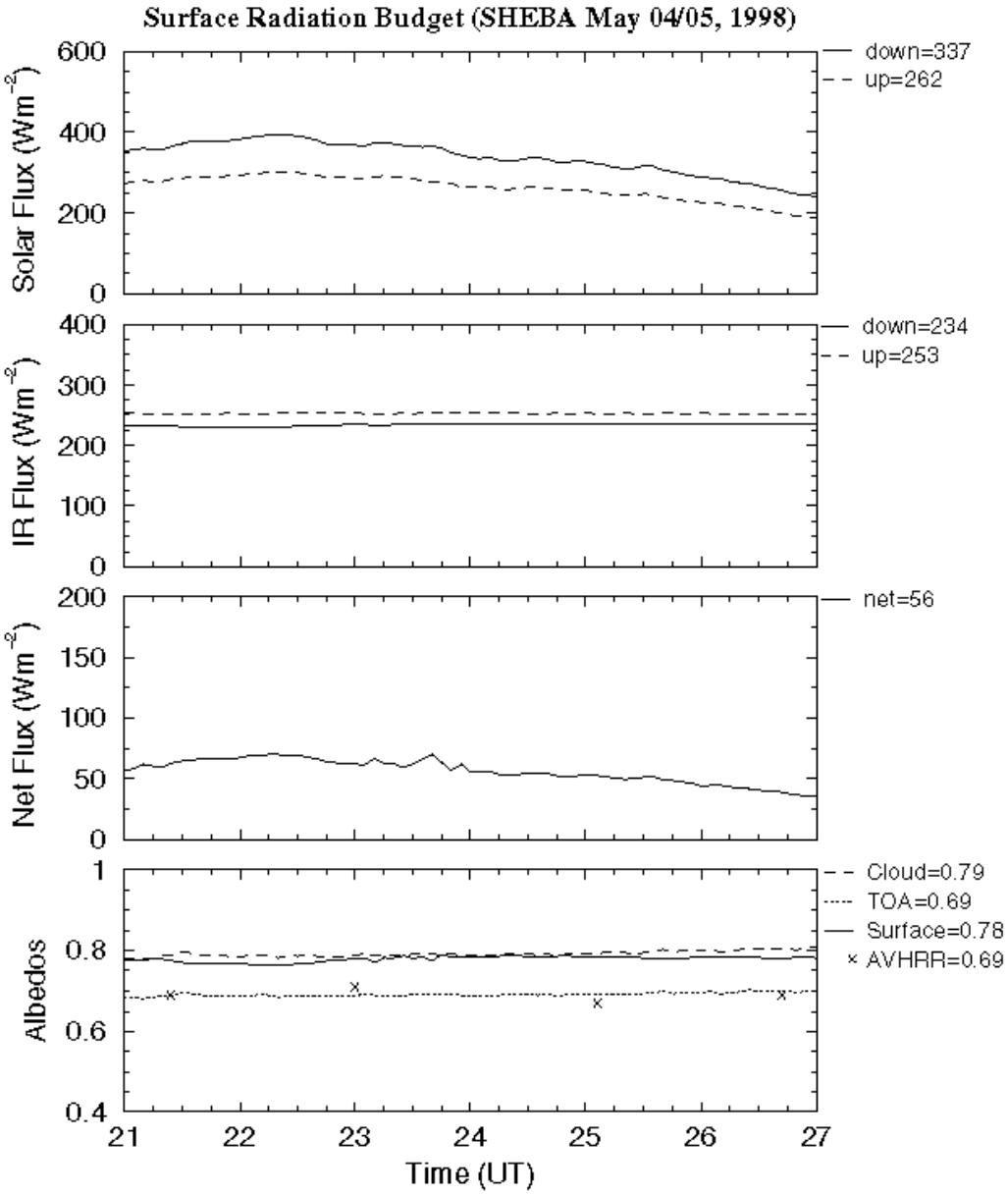
Surface Radiation Budget (SHEBA May 04/05, 1998)
Solar Flux (Wm-2)
600
400
200
0
down=337
up=262
IR Flux (Wm-2)
400
300
200
100
0
down=234
up=253
Net Flux (Wm-2)
200
150
100
50
0
net=56
Albedos
1
0.8
0.6
0.4
Cloud=0.79
TOA=0.69
Surface=0.78
AVHRR=0.69
21
22
23
24
25
26
27
Time (UT)

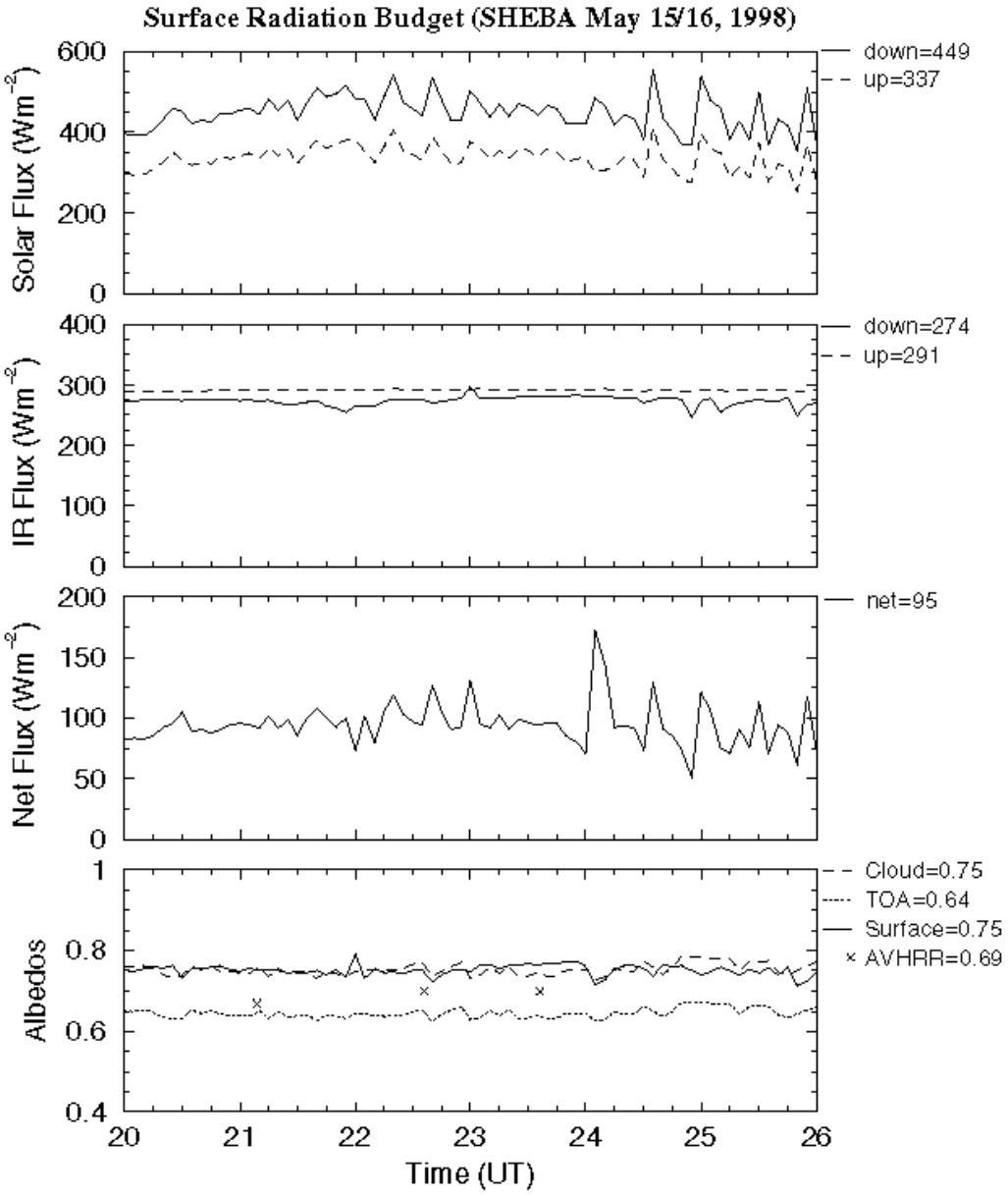
Surface Radiation Budget (SHEBA May 15/16, 1998)
Solar Flux (Wm-2)
600
400
200
0
down=449
up=337
IR Flux (Wm-2)
400
300
200
100
0
down=274
up=291
Net Flux (Wm-2)
200
150
100
50
0
net=95
Albedos
1
0.8
0.6
0.4
Cloud=0.75
TOA=0.64
Surface=0.75
AVHRR=0.69
20
21
22
23
24
25
26
Time (UT)

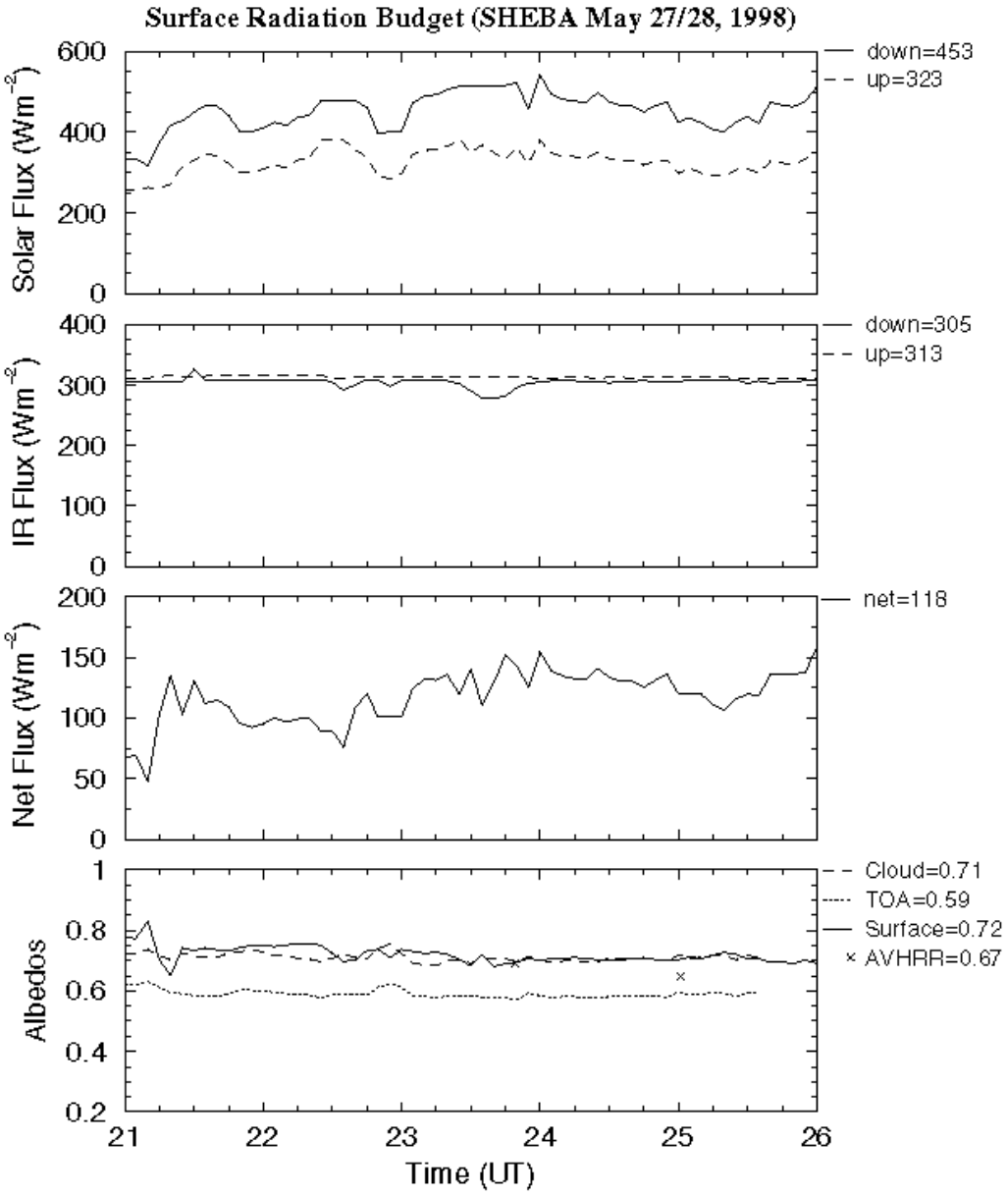
Surface Radiation Budget (SHEBA May 27/28, 1998)
Solar Flux (Wm-2)
600
400
200
0
down=453
up=323
IR Flux (Wm-2)
400
300
200
100
0
down=305
up=313
Net Flux (Wm-2)
200
150
100
50
0
net=118
Albedos
1
0.8
0.6
0.4
0.2
Cloud=0.71
TOA=0.59
Surface=0.72
AVHRR=0.67
21
22
23
24
25
26
Time (UT)

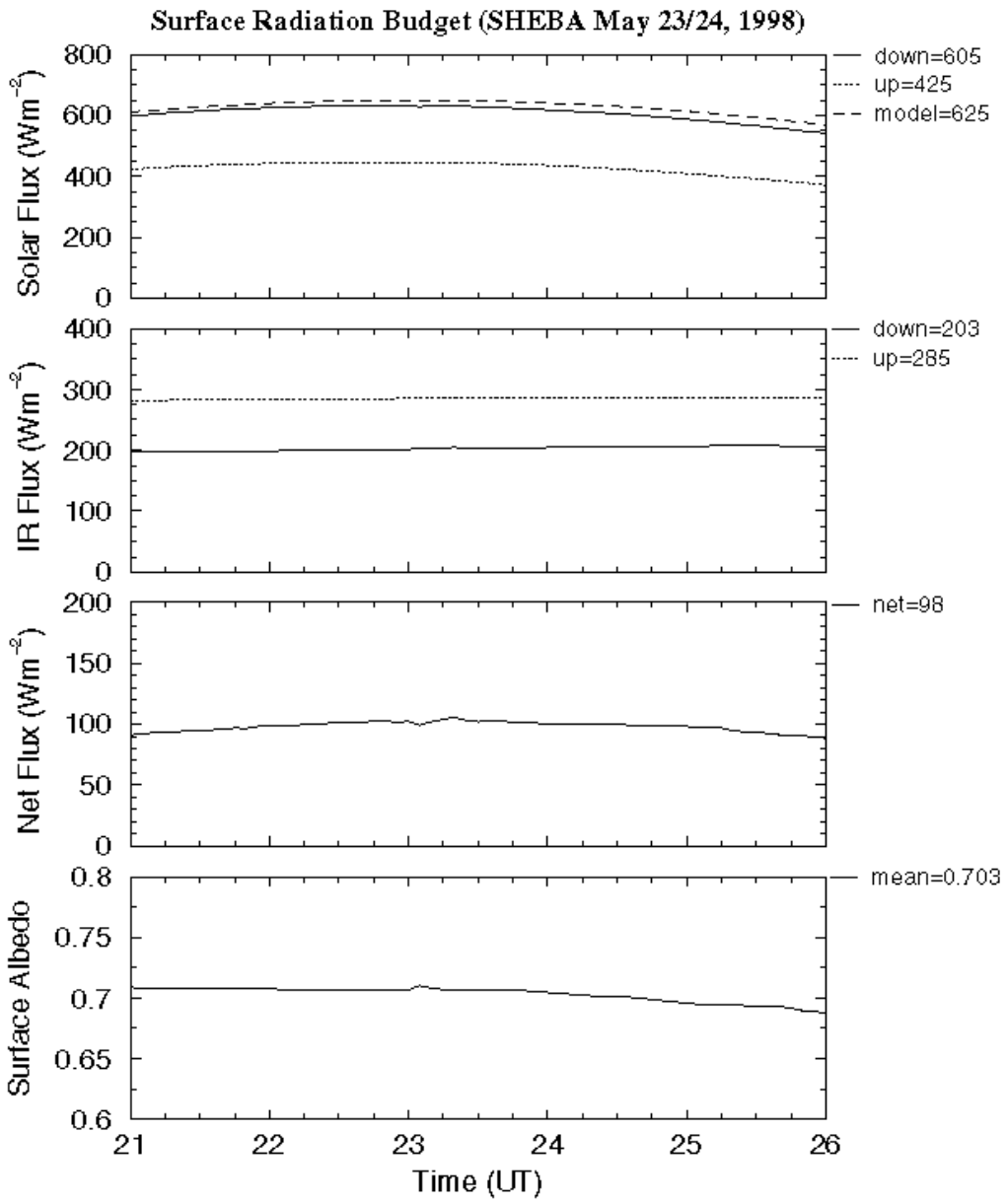
Surface Radiation Budget (SHEBA May 23/24, 1998)
Solar Flux (Wm-2)
800
600
400
200
0
down=605
up=425
model=625
IR Flux (Wm-2)
400
300
200
100
0
down=203
up=285
Net Flux (Wm-2)
200
150
100
50
0
net=98
Surface Albedo
0.8
0.75
0.7
0.65
0.6
mean=0.703
21
22
23
24
25
26
Time (UT)

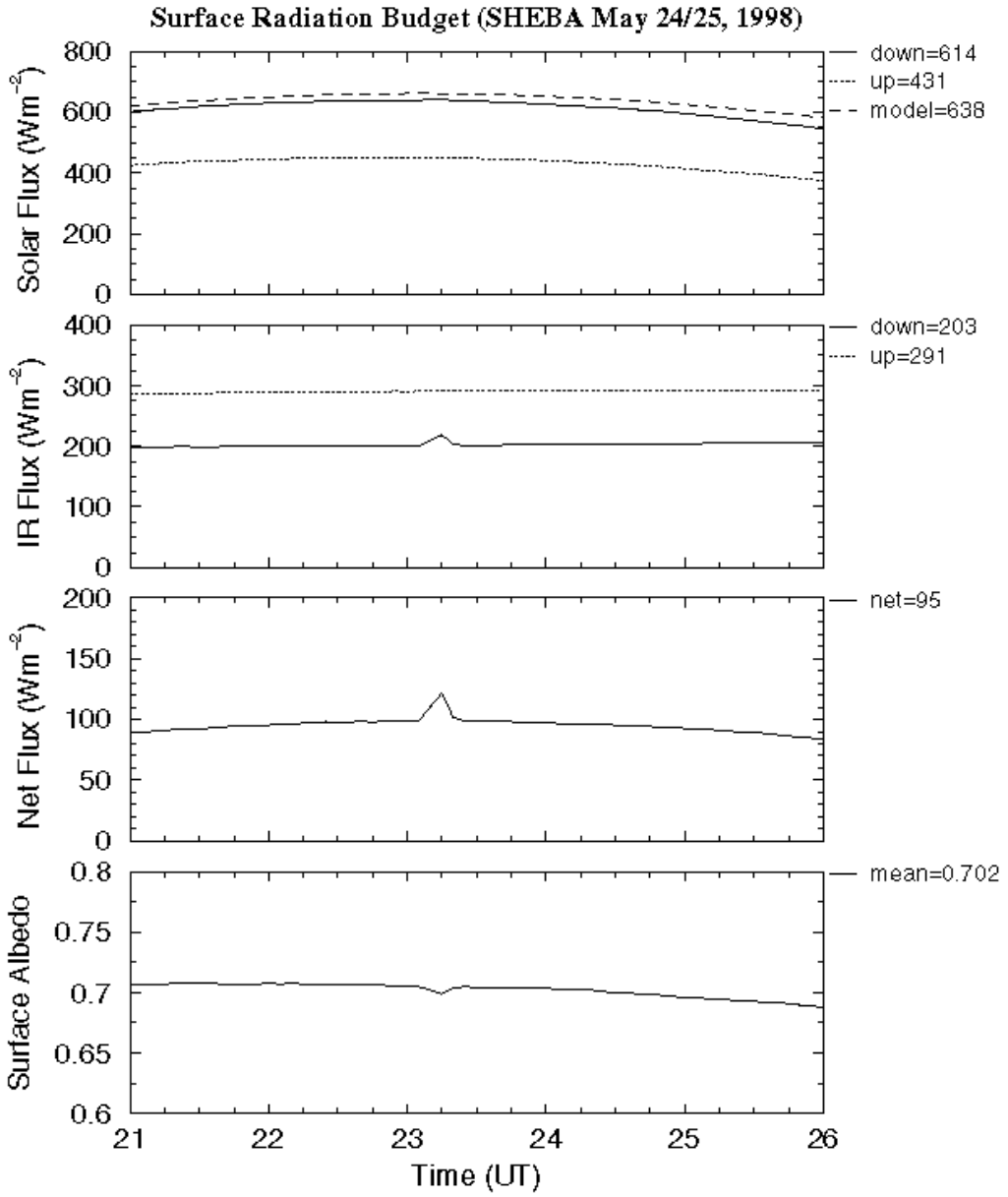
Surface Radiation Budget (SHEBA May 24/25, 1998)
Solar Flux (Wm-2)
800
600
400
200
0
down=614
up=431
model=638
IR Flux (Wm-2)
400
300
200
100
0
down=203
up=291
Net Flux (Wm-2)
200
150
100
50
0
net=95
Surface Albedo
0.8
0.75
0.7
0.65
0.6
mean=0.702
21
22
23
24
25
26
Time (UT)